

# International Conference on Space Optics—ICSO 2014

La Caleta, Tenerife, Canary Islands

7–10 October 2014

*Edited by Zoran Sodnik, Bruno Cugny, and Nikos Karafolas*



## *Space active optics sensing and control for earth observation at high angular resolution*

*C. Escolle*

*V. Michau*

*M. Ferrari*

*T. Fusco*

*et al.*



International Conference on Space Optics — ICSO 2014, edited by Zoran Sodnik, Nikos Karafolas, Bruno Cugny, Proc. of SPIE Vol. 10563, 105635U · © 2014 ESA and CNES  
CCC code: 0277-786X/17/\$18 · doi: 10.1117/12.2304137

## SPACE ACTIVE OPTICS SENSING AND CONTROL FOR EARTH OBSERVATION AT HIGH ANGULAR RESOLUTION

C. Escolle<sup>1</sup>, V. Michau<sup>2</sup>, M. Ferrari<sup>1</sup>, T. Fusco<sup>1,2</sup>, E. Hugot<sup>1</sup>, T. Bret-Dibat<sup>3</sup>.

<sup>1</sup>Aix-Marseille University, CNRS, LAM, UMR 7326, 13388, Marseille, France. <sup>2</sup>Onera – The French Aerospace Lab, 92322 Chatillon, France. <sup>3</sup>Cnes– Centre National d'Etudes spatiales, 31000 Toulouse, France

### I. INTRODUCTION:

Discoveries in astronomy and earth science lie on the capabilities of the space observatories to see fainter objects and smaller details. This need of high collecting power and high angular resolution implies instruments with large primary mirrors. However, a simple scaling of existing space telescopes leads to bigger optical elements and structure that exceed the allocated volume and launch mass capability of medium size launchers. Due to volume, weight and cost constraints on satellites, the next generation of large telescopes must combine innovative and compact optical concepts [1] using lightweight primary mirrors and structures [2]. Furthermore the lightweighting of primary mirrors and structures reduce their stiffness and make them more deformable under static and dynamic load. Also, the compactness needed implies primary mirrors with low focal ratio and a small distance between primary and secondary mirrors. This leads to an optical train more sensitive to misalignment [1].

The harsh satellite environment such as thermal gradient during orbit, gravity load difference between ground and space, as well as vibrations during launch lead to primary mirror optical surface deformations, telescope structure deformations and misalignments of the secondary mirror. All these perturbations degrade the telescope optical performance. Moreover, it may be more and more difficult for satellite and instrument manufacturers to run complete tests on ground, because of the gravity deformations of the large optics that cannot be corrected easily. Therefore, optimal image quality recovery and in flight alignment require active optics and structures to compensate in situ the wave front distortions. A space active optics system mostly consists of a wave front measurement system, a correcting system and a control system. The control system should ensure a maximum information extraction about perturbations from measurements in order to correct efficiently with respect to the correcting system capabilities.

The wave front measurement problem for space active optics as already been addressed in [3] and [4]. Moreover, [5] shows that the problem of perturbations reconstruction and correction can be processed separately without performance loss. Thus, this paper focuses on the way to optimally estimate the perturbations from the measurements. The estimation performance directly impacts the final optical quality of the telescope. In the following, we compare the performances of a Minimum Mean Square Error (MMSE) estimator [5] and a classical Least Square (LS) estimator. The MMSE is an optimal estimator used in Multi Conjugate Adaptive Optics (MCAO).

In Sec. II, we present the telescope optical model and the perturbations statistic model that we use to simulate the telescope optical quality degradation. Then, we explain how we implement it in our active optics system model. In Sec. III, we describe the measurement and correction systems used in our model. Then, we expressed the MMSE and LS estimators associated with our assumptions on the perturbations and correcting system characteristics. Then we derive the estimation error for both estimators. In Sec. IV, we show the results in terms of residual wave front in the exit pupil of the telescope and we compare the performances of MMSE and LS estimators.

### II. PERTURBATIONS MODEL:

We choose a three mirrors anastigmatic Korsch telescope [6] as basis optical concept for this study. This concept is a classical optical configuration for space telescope (JWST, Euclid, Pleiades). In our case, the advantage of this configuration is the real exit pupil in which we can put a correcting mirror. The primary mirror (optical entrance pupil) is a lightweighted parabolic concave mirror with a diameter of 1.5 m and a radius of curvature of 3.6 m. The secondary mirror is a convex elliptic mirror with a diameter of 0.36 m and a radius of curvature of 1 m. The third mirror is a concave elliptic mirror with a diameter of 0.5 m and a radius of curvature of 1.3 m. Fig. 1 shows a scheme of the optical model used in this paper.

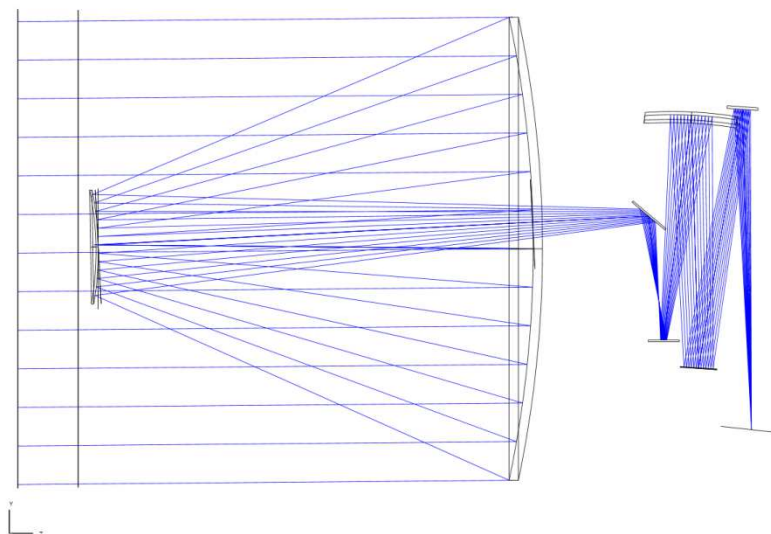


**Fig. 1.** 2D sketch of the studied space telescope optical design

In this paper we consider only the perturbations encountered by the instrument at the beginning of its lift in orbit. During launch the satellite experiences harsh vibrations which may move optical elements. Moreover, the gravity and thermal difference between space environment and the integration and alignment conditions lead to deformations of the lightweighted primary mirror and the low stiffness telescope structure.

The structure deformations and launch vibration imply optical elements displacements. The misalignments coming from these displacements degrade the telescope final image quality. A quick sensitivity study of the optical design shows that the secondary mirror is ten times more sensitive than the other mirrors. Thus only the secondary mirror displacements have been considered in the following study. The primary mirror has been chosen as reference and has been considered fixed.

The deformations of a primary mirror coming from gravity release and the optimization of these deformations has been studied in [7]. We use the result of this paper as an input for the primary mirror deformations considered in our study.

We use an optical ray tracing software (Zemax) to implement the optical model of the space telescope and to introduce the perturbations of the secondary and primary mirrors. For the secondary mirror, we consider the displacement over the optical axis (Z axis), and the two orthogonal axes (X and Y). We consider also, the tilt around X and Y axes. For the introduction of the primary mirror deformations we use a specific surface type in Zemax. This surface type can define the mirror's optical surface with a conicoid surface plus Zernike polynomials. We consider only the first hundred polynomials without piston and tilts i.e. from  $Z_4$  to  $Z_{103}$  in Noll numbering.

We assume that the perturbations coming from the secondary and primary mirrors follow a Gaussian statistic with a zero mean value. The standard deviations for each perturbation have been showed on Fig.2. We generate the random perturbations from these statistic data.

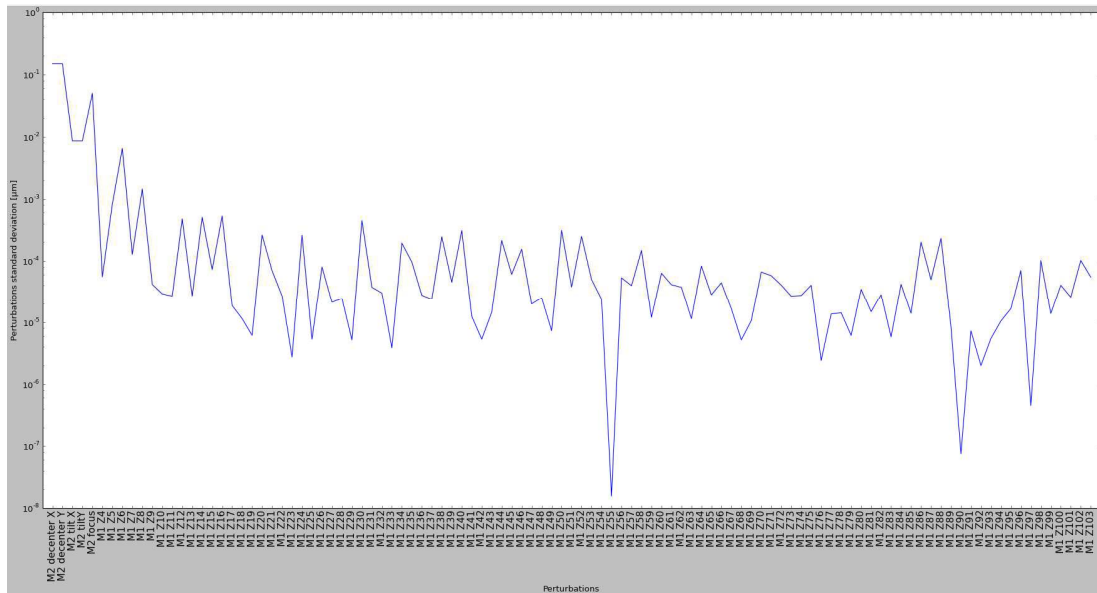


Fig. 2. Perturbations standard deviation

### III. LOOP MODEL:

We see in the previous section that the phase perturbations have been located in the pupil and the secondary mirror plans. In order to reach the best performance in the all the Field Of View (FOV), the correcting system should be in the same plan as the perturbations or in an optically conjugated plan. Thus we consider a correcting system as follow:

- A 5 Degree of Freedom (DoF) system on  $M_2$  to correct decentres, tilts and focus of this mirror.
- A deformable mirror in the external pupil to correct the primary mirror deformation. The deformable mirror is assumed to be perfectly conjugated with the primary. We have checked the validity of this assumption considering the amplitude of  $M_2$  decentring.

The measurement system consists of two Wave Front Sensors (WFS). Each WFS measure the wave front in a different FOV direction. Only this kind of configuration allows us to reconstruct and separate the perturbations coming from the primary and secondary mirror. The vector describing  $M_1$  deformations and  $M_2$  displacements is denoted  $\psi$ . The wave front perturbation induced by  $\psi$ , as seen by the WFS is denoted  $\phi$ . The wave front perturbation induced by  $\psi$ , as seen by the WFS is denoted  $\phi$ . It may be written as:  $\phi = M\psi$ .  $M$  is the interaction matrix of the system. It represents the link between the perturbations coming from the primary and secondary mirrors and the wave front sensing measurements in the different FOV directions.

This configuration with two layers of perturbation, two correcting set ups conjugated and measurements in several FOV directions sounds like an ideal MCAO configuration. Therefore, we apply an MCAO optimal wave front reconstructor. The derivation of the MMSE estimator can be found in [5]. The final result for the expression of the reconstruction matrix is

$$W_{rec} = C_\phi M^T [MC_\phi M^T + C_n]^{-1} \quad (1)$$

where  $C_\phi$  and  $C_n$  are the perturbations and noise covariance matrices, and  $T$  superscript symbol denotes the transpose matrix. For comparison, we consider also the reconstruction matrix in the classical case of a least square estimator

$$W_{rec} = M^\dagger \quad (2)$$

where  $\dagger$  superscript symbol denotes the generalized inverse matrix. In the next section, we show comparison results between these two estimators.

The wave front of correction in the exit pupil of the telescope can be written as

$$\hat{\phi} = MW_{rec}(\phi + n) \quad (3)$$

where  $\phi$  is the true phase in the exit pupil of the telescope and  $n$  the measurement noise. Then the mean square error of the wave front after correction can be expressed as

$$\epsilon = \langle \|\hat{\phi} - \phi\|^2 \rangle \quad (4)$$

where  $\langle \rangle$  stands for the mathematical expectation on both perturbations and noise,  $\|\cdot\|^2$  denotes the norm in the wave front space. The mean square error characterises the performance of an estimator and we choose it as performance criterion. Putting Eq. (3) in Eq. (4) yields

$$\epsilon = \langle \|(MW_{rec} - I)\phi + MW_{rec}n\|^2 \rangle \quad (5)$$

where  $I$  denotes the identity matrix. If we express  $MW_{rec}$  in the case of the MMSE estimator

$$MW_{rec} = MC_{\phi}M^T[MC_{\phi}M^T + C_n]^{-1} = [I + C_n(MC_{\phi}M^T)^{-1}]^{-1}.$$

We can see that in a low noise case, ( $n \ll \phi$ )  $MW_{rec}$  go to the identity matrix. Thus the mean square error converges to the noise variance. On the contrary, in the high noise case,  $MW_{rec}$  go to null matrix and the mean square error approaches the true wave front variance. Another way to understand it is when noise increase, the reconstructed wave front approaches zero and the MMSE mean square error is the true wave front variance.

We implement these wave front estimators in Python. Firstly, we use the PyZDDE toolbox [8] and the Dynamic Data Exchange (DDE) capabilities of Zemax to process the interaction matrix. We compute the random perturbation values with statistics presented Sec. II. Then we calculate the exit pupil wave front error coming from the perturbations and we expand it over a Zernike polynomials basis. We do that for the two different FOV directions of the WFS. We add a Gaussian noise to these wave fronts to simulate real measurements. To define the noise model parameters, we assume that the measurements have been done by Shack-Hartmann WFSs. We use noise propagation coefficient from [9] to compute the noise spectrum with respect to the Zernike polynomials radial order. From these noisy measurements, we estimate the perturbations with the MMSE and LS estimators. Finally we compute the estimated wave front in the exit pupil in order to calculate the performance criterion of the estimators. Fig. 3 shows a block diagram of this process.

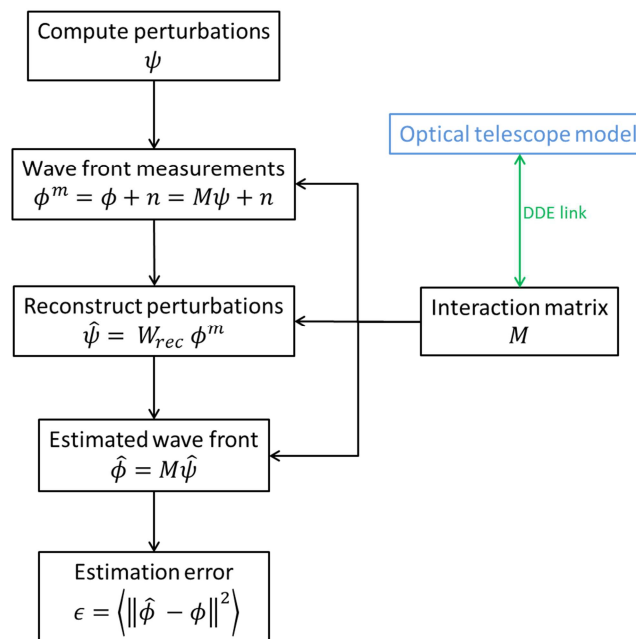
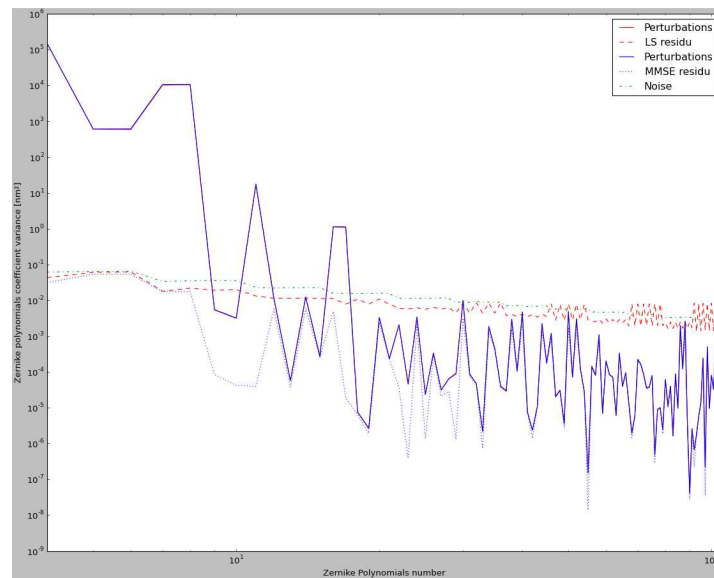


Fig. 3. Active optics simulation Block diagram

#### IV. RESULTS:

In the next section, we present a comparison of the two estimators developed in the previous section. Firstly we show the performance in terms of residual wave front in a medium noise case. Fig. 4 shows the Zernike polynomial coefficients variance with respect to the Zernike polynomial number. The solid lines (red and blue) represent the wave front distortion in the exit pupil coming from the random perturbations of primary and secondary mirrors. There are two curves because the perturbation generation is a random process but both curves are nearly confounded. The dash-dot line (green) shows the noise level. The dash line (red) shows the

residual wave front error variance for the LS estimator. The residual wave front can be expressed as  $\phi_{res} = \hat{\phi} - \phi$ . Finally the dot line (blue) represents the residual wave front error variance for the MMSE.



**Fig. 4.** Zernike polynomial variance versus Zernike polynomial number for perturbation (Blue and red solid line), noise (green dash dot line), LS residue (red dash line) and MMSE residue (blue dot line)

To analyse these results we define the Signal to Noise Ratio (SNR) as  $NR = trace(C_{\phi})/trace(C_n)$ . We can separate the previous figure in two parts. In the left part of the graphic, the SNR is high ( $SNR > 10^4$ ), both estimators have the same performance and the residual variance follows the noise variance curve. In the right part of the graphic, the SNR decrease down to  $10^{-4}$ , MMSE follow the perturbations variance and thus have better performance than LS solution. On the contrary, the LS estimator continues to follow the noise variance curve. This behaviour is a qualitative illustration in a working case of the estimators' behaviour foreseen in the previous section.

The Fig. 5 gives more quantitative information about the estimators' performances. It shows the variations of the mean square error for each estimator with respect to the SNR. The solid line represents the perturbations variance. The behaviour expected from the expression of the mean square error derived in the Sec. III, can be observe on the previous graphic.

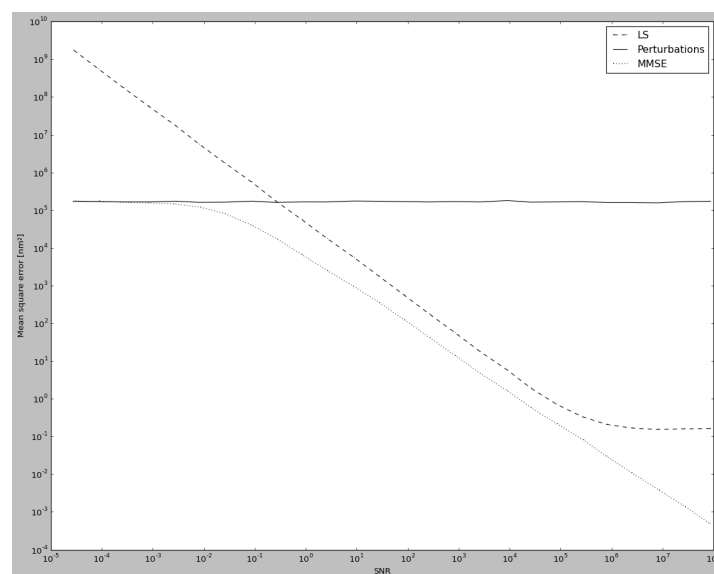


**Fig. 5.** Mean square error versus SNR for the LS (dash line) and the MMSE estimators (dot line)

From the Fig. 5 we can conclude that the MMSE has always better performance than the LS estimator. To reach a few nanometres error on the estimated wave front we need a SNR value around  $10^4$ . At this SNR the difference of performance between the LS and MMSE estimator represents a factor 5.

## V. CONCLUSION:

In this paper, we start from the perturbations of a next generation space telescope when it begins its in-flight operation. Alignment and optimal image quality recovering is a major part of the commissioning phase. In this context, we present an optimal wave front estimator to reconstruct these perturbations and to separate those coming from the primary and secondary mirrors. This optimal approach derives from a MMSE estimator that minimizes the mean residual wave front error in the exit telescope pupil. It corresponds to a tomographic reconstruction of the perturbations.

Then we compare the MMSE estimator with a LS estimator. We show that the MMSE estimator's performance is always better than the LS one whatever the measurement noise level. But the differences in term of mean square error increase when the SNR decrease.

In the present paper we only consider the behaviour of the MMSE estimator with respect to the noise level. Future work should be developed on two axes. In a first step at short time scale, the study of the influence of the WFS position in the FOV. In a second step at a longer time scale, we need to take account of the correction system performance to have a complete active optics loop simulation.

## ACKNOWLEDGEMENT

This study is performed with the support of a Ph.D. grant from CNES (Centre National d'Etudes Spatiales) and ONERA (The French Aerospace Lab).

## REFERENCES

- [1] V. Costes, G. Cassar, and L. Escarrat, "Optical design of a compact telescope for next generation earth observation systems," in *Proc. ICSO*, 2012.
- [2] L. Feinberg et al, "Space telescope design considerations," *Optical Engineering*, vol. 51. 2012.
- [3] A. Montmerle Bonnefois et al., "Comparative theoretical and experimental study of a Shack-Hartmann and a Phase Diversity Sensor, for high-precision wavefront sensing dedicated to Space Active Optics", this conference.
- [4] A. Liotard et al, "Wave-front sensing for space active optics: rascasse project," this conference.
- [5] T. Fusco, JM. Conan, G. Rousset, L. M. Mugnier and V. Michau, "Optimal wave-front reconstruction strategies for multiconjugate adaptive optics," *J. Opt. Soc. Am*, vol. 18. 2001.
- [6] D. Korsch, "Closed-form solutions for imaging systems, corrected for third-order aberrations," *J. Opt. Soc. Am* 63 (6), 1973.
- [7] C. Escolle et al, "Adapting large lightweight primary mirror to space active optics capabilities," in *Proc. SPIE*, 2014.
- [8] <https://github.com/indranilsinharoy/PyZDDE>
- [9] F. Rigaut and E. Gendron, "Laser guide star in adaptive optics: the tilt determination problem," *Astron. Astrophys.* 261, 1992.